RESEARCH ARTICLE SUMMARY

NUCLEIC ACID ORIGAMI

Single-stranded DNA and RNA origami

Dongran Han,* Xiaodong Qi,* Cameron Myhrvold, Bei Wang, Mingjie Dai, Shuoxing Jiang, Maxwell Bates, Yan Liu, Byoungkwon An,† Fei Zhang,† Hao Yan,† Peng Yin†

INTRODUCTION: Self-folding of an information-carrying polymer into a compact particle with defined structure and function (for example, folding of a polypeptide into a protein) is foundational to biology and offers attractive potential as a synthetic strategy. Over the past three decades, nucleic acids have been used to create a variety of complex nanoscale shapes and devices. In particular, multiple DNA strands have been designed to self-assemble into user-specified structures, with or without the help of a long scaffold strand. In recent years, RNA has also emerged as a unique, programmable material, offering distinct advantages for molecular self-assembly. On the other hand, biological macromolecules, such as proteins (or protein domains), typically fold from a single polymer into a well-defined compact structure. The ability to fold de novo designed nucleic acid nanostructures in a similar manner would enable unimolecular folding instead of multistrand assembly and even replication of such structures. However, a general strategy to construct large [>1000 nucleotides (nt)] single-stranded origami (ssOrigami) remains to be demonstrated where a single-stranded nucleic acid folds into a user-specified shape.

RATIONALE: The key challenge for constructing a compact single-stranded structure is to achieve structural complexity, programmability, and generality while maintaining the topological simplicity of strand routing (to avoid putative kinetic traps imposed by knots) and hence ensuring smooth folding. The key innovation of our study is to use partially complemented double-stranded DNA or RNA and parallel crossover cohesion to construct such a structurally complex yet knot-free structure that can be folded smoothly from a single strand.

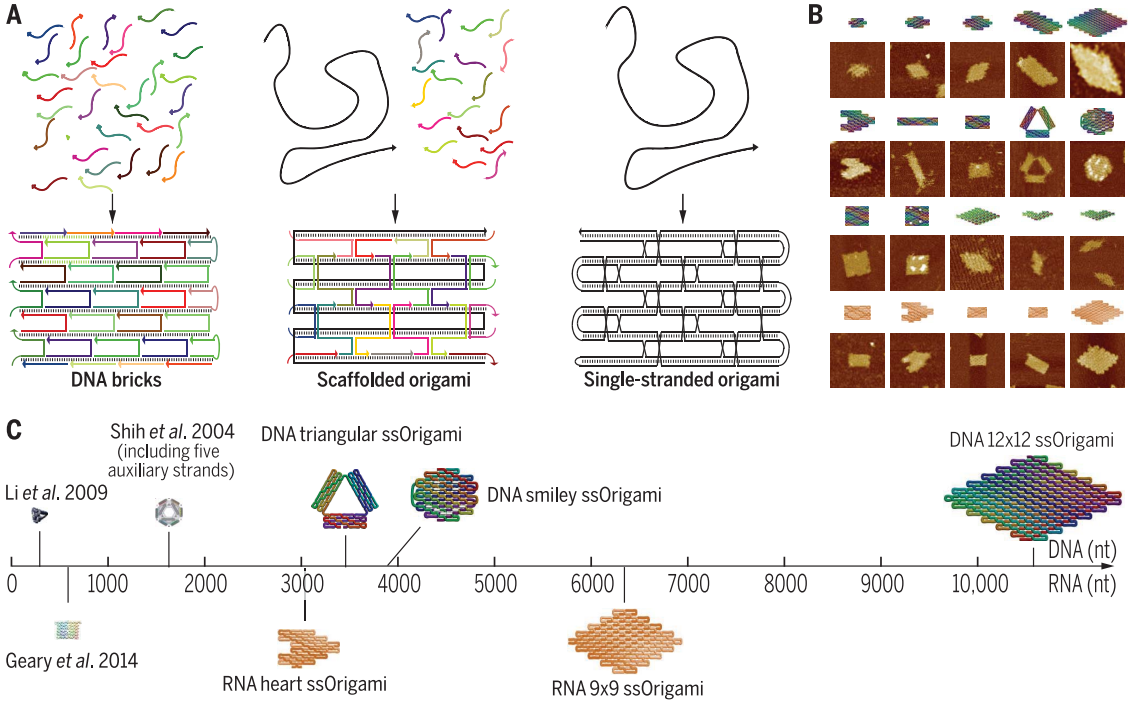
RESULTS: Here, we demonstrate a framework to design and synthesize a single DNA or RNA strand to efficiently self-fold into an unknotted compact ssOrigami structure that approximates an arbitrary user-prescribed target shape. The generality of the method was validated by the construction of 18 multikilobase DNA and 5 RNA ssOrigami, including a ~10,000-nt DNA structure (37 times larger than the previous largest discrete single-stranded DNA nanostructure) and a ~6000-nt RNA structure (10 times larger than the previous largest RNA structure). The raster-filling nature of ssOrigami permitted the experimental construction of programmable patterns of markers (for example, a "smiley" face) and cargoes on its surface, its single-strandedness enabled the demonstration of facile replication of the strand in vitro and in living cells, and its programmability allowed us to codify the design process and develop a web-based automated design tool.

ON OUR WEBSITE

Read the full article at http://dx.doi.org/10.1126/science.aao2648

CONCLUSION: The work here establishes that unimolecular DNA or RNA folding, similar to multicomponent self-assembly, is a fundamental, general, and practically tractable strategy for constructing user-specified and replicable nucleic acid nanostructures, and expands the design space and material scalability for bottom-up nanotechnology. ■

The list of author affiliations is available in the full article online.
*These authors contributed equally to this work.
†Corresponding author. Email: py@hms.harvard.edu (P.Y.); hao.yan@asu.edu (H.Y.); fei.zhang@asu.edu (F.Z.); dran@csail.mit.edu (B.A.)
Cite this article as D. Han *et al.*, *Science* **358**, eaao2648 (2017). DOI: 10.1126/science.aao2648



Folding of DNA or RNA ssOrigami structures. (**A**) Multiple DNA strands have been designed to self-assemble without (left) or with (middle) a long scaffold strand. Here, we fold single long DNA or RNA strands into target shapes (right). (**B**) Schematics and atomic force microscopy images of single-stranded DNA (top three rows) and RNA (bottom row) nanostructures. (**C**) Size comparison between ssOrigami and previously reported single-stranded nucleic acid nanostructures.

Downloaded from https://www.science.org on November 16, 2023

RESEARCH ARTICLE

NUCLEIC ACID ORIGAMI

Single-stranded DNA and RNA origami

Dongran Han,[1,2]* Xiaodong Qi,[3,4]* Cameron Myhrvold,[1,2] Bei Wang,[2,5] Mingjie Dai,[1,2] Shuoxing Jiang,[3,4] Maxwell Bates,[6] Yan Liu,[3,4] Byoungkwon An,[6]† Fei Zhang,[3,4]† Hao Yan,[3,4]† Peng Yin[1,2]†

Self-folding of an information-carrying polymer into a defined structure is foundational to biology and offers attractive potential as a synthetic strategy. Although multicomponent self-assembly has produced complex synthetic nanostructures, unimolecular folding has seen limited progress. We describe a framework to design and synthesize a single DNA or RNA strand to self-fold into a complex yet unknotted structure that approximates an arbitrary user-prescribed shape. We experimentally construct diverse multikilobase single-stranded structures, including a ~10,000-nucleotide (nt) DNA structure and a ~6000-nt RNA structure. We demonstrate facile replication of the strand in vitro and in living cells. The work here thus establishes unimolecular folding as a general strategy for constructing complex and replicable nucleic acid nanostructures, and expands the design space and material scalability for bottom-up nanotechnology.

Foundational to biological replication, function, and evolution is the transfer of information between sequence-specific polymers (for example, DNA replication, RNA transcription, and protein translation) and the folding of an information-carrying polymer into a compact particle with defined structure and function (for example, protein and RNA folding). Biology's operational principles on the molecular scale motivate synthetic efforts to design replicable, information-bearing polymers that can self-fold into user-prescribed nanoscale shapes.

Using nucleic acids' specific base pairing, complex nanostructures have been created with DNA and RNA (*1*–*27*), enabling diverse applications (*28*–*40*). Particularly noteworthy are multikilobase, megadalton-scale nanoparticles with arbitrary user-prescribed geometry that are self-assembled from hundreds of synthetic DNA strands, with and without the assistance of a central organizing scaffold strand [that is, scaffolded DNA origami (*4*, *8*–*10*, *13*, *20*–*23*) and DNA bricks (*14*, *15*)]. In contrast to the remarkable success of structures self-assembled from multiple components, the progress on designing a single-stranded DNA (ssDNA) or RNA (ssRNA) that can self-fold into a defined shape is limited, and only relatively simple shapes were demonstrated [for example, the folding of a 79–nucleotide (nt) DNA strand into a four-arm junction (*41*), a 160-nt strand into a paranemic crossover (*42*), a 286-nt DNA strand into a tetrahedron (*43*), and a 660-nt RNA into a six-helix rectangle tile (*44*)]. In addition, a 1669-nt DNA strand, with the help of five auxiliary strands, was folded into an octahedron structure (*3*). Notably, the simple ssDNA structures (*41*–*43*) as well as the 1669-nt scaffold for the octahedron (*3*) can be replicated in vitro (*3*, *41*–*43*), and these simple single-stranded structures were cloned and replicated in living cells (*43*, *45*). The 660-nt RNA structure can be transcribed from a DNA template and folds isothermally (*44*).

The ability to design a nucleic acid polymer that self-folds in a protein-like fashion into a user-prescribed compact shape not only is interesting and important on a fundamental basis but also offers key conceptual advantages in practicality (*3*, *41*–*45*) over the current paradigm of multicomponent DNA self-assembly. Compared to multistranded DNA structures formed via self-assembly, ssDNA nanostructures formed via self-folding offer greater potential of being amplifiable, replicable, and clonable, and hence the opportunity for cost-efficient, large-scale production using enzymatic and biological replication, as well as the possibility for using in vitro evolution to produce sophisticated phenotypes and functionalities. In addition, unimolecular folding process is independent of the reactant concentration and thus, in principle, offers higher formation yield and more robust folding kinetics than multistranded structures produced with concentration-dependent intermolecular self-assembly. Furthermore, unlike multistranded DNA nanostructures, which typically contain dozens or hundreds of distinct components and often undesirable defects such as missing or incorrectly incorporated or synthesized component strands, a single-stranded structure could, in principle, be synthesized as a homogeneous system with high purity [for example, via enzymatic production of monoclonal strands (*46*)].

Despite its fundamental importance and practical desirability, as well as the aforementioned promising early efforts (*3*, *41*–*45*), it remains challenging to develop a general strategy for the design and synthesis of an ssDNA or ssRNA that can fold into a user-prescribed complex, arbitrary shape [for example, comparable in complexity and programmability to scaffolded DNA origami (*4*)]. The key design challenge is to achieve structural complexity, programmability, and generality while maintaining the topology simplicity of strand routing (to avoid kinetic traps imposed by knots) and hence ensuring smooth folding. This challenge arguably restricts the size of the current largest ssDNA structure to 286 nt with a relatively simple and porous tetrahedron shape (*43*) and underlies the use of five auxiliary strands for the proper formation of the largely but not entirely single-stranded 1669-nt DNA octahedron (*3*).

We introduce here a general design and synthesis framework for folding a multikilobase ssDNA strand into a complex user-prescribed shape. The key innovation is to use partially complemented double-stranded DNA (dsDNA) and parallel crossover cohesion (*3*, *47*–*50*) to construct a structurally complex yet knot-free structure that can be folded smoothly from a single strand. We call these structures ssDNA origami or DNA ssOrigami. We experimentally validated the versatility of the strategy by constructing a variety of space-filling, compact shapes (for example, different-sized rhombus, rectangle, square, disc, heart, and triangle shapes; 18 shapes in total). The space-filling nature of the structure and the unique base-resolution addressability along the strand enabled us to create user-prescribed patterns of protruding hairpins or loops on the structure surface (for example, a pattern mimicking a "smiley" face was experimentally demonstrated), and such loops can and were used as "handles" to attach other moieties. The strategy produces structures with an architecture that is amenable to amplification and replication; we experimentally demonstrated that a folded ssOrigami structure can be melted and used as a template for amplification by polymerases in vitro and that the ssOrigami strand can be replicated and amplified via clonal production in living cells. The design is scalable, as validated by the experimental construction of a 10,682-nt rhombus shape, which is 37 times larger than the previous largest ssDNA structure (*43*) and 16 times larger than the previous largest ssRNA structure (*44*), and approaches the complexity of scaffolded DNA origami (*4*).

Strikingly, the design for DNA ssOrigami can be readily adapted to produce complex ssRNA nanostructures (that is, RNA ssOrigami) with

[1]Department of Systems Biology, Harvard Medical School, Boston, MA 02115, USA. [2]Wyss Institute for Biologically Inspired Engineering, Harvard University, Boston, MA 02115, USA. [3]Biodesign Center for Molecular Design and Biomimetics Biodesign Institute, Tempe, AZ 85287, USA. [4]School of Molecular Sciences, Arizona State University, Tempe, AZ 85287, USA. [5]Department of Polymer Science and Engineering, University of Science and Technology of China, Hefei, Anhui 230026, P. R. China. [6]BioNano Research Group, Autodesk Life Sciences, Pier 9, San Francisco, CA 94111, USA.
*These authors contributed equally to this work.
†Corresponding author. Email: py@hms.harvard.edu (P.Y.); hao.yan@asu.edu (H.Y.); fei.zhang@asu.edu (F.Z.); dran@csail.mit.edu (B.A.)

Downloaded from https://www.science.org on November 16, 2023

minimal adjustment. RNA has been used to construct synthetic nanostructures (*44*, *51*–*54*) and offers unique application potentials over DNA structures (for example, functional diversity, economical production via genetic expression, and amenability for intracellular applications) (*44*). However, whereas multikilobase, megadalton-size discrete DNA nanostructures have been demonstrated [for example, via scaffolded origami (*4*, *8*) and DNA bricks (*14*, *15*)], synthetic RNA nanostructures remain comparatively simple: The largest discrete structure demonstrated is the aforementioned 660-nt ssRNA tile (*44*). We successfully adapted our DNA ssOrigami design to RNA by merely slightly adjusting the design parameter to account for the helical periodicity difference between DNA and RNA duplex, and produced a variety of multikilobase complex RNA ssOrigami structures with user-prescribed shapes (for example, rhombus, rectangle, and heart shapes), including a 6337-nt RNA structure that represents a 10-fold increase in complexity for RNA nanotechnology. The generality and adaptability of the ssOrigami architecture is additionally revealed by the successful folding of two identical target shapes by both the sense and antisense RNA strands transcribed from the same dsDNA template.

The programmability of the ssOrigami architecture further allows us to codify the design process as a mathematically rigorous formal algorithm and automate the design by developing a user-friendly software tool, which takes as input an arbitrary space-filling shape and produces as output a DNA strand that folds into the shape in a knot-free fashion. The algorithm and software was validated by the automated design and experimental construction of six distinct DNA ssOrigami structures (four rhombus and two heart shapes).

The ssOrigami work establishes that it is possible to design a multikilobase ssDNA or ssRNA to fold into a user-prescribed complex shape. It produces single-component DNA nanostructures with complexity comparable to those assembled from hundreds of components and increases the structural complexity for designable RNA nanotechnology. Unimolecular folding, alongside self-assembly (for example, scaffolded DNA origami and DNA bricks), thus represents another fundamental, general, yet practically accessible design strategy for constructing digitally programmable nanostructures and expands the design space and material scalability for bottom-up nanotechnology.

Design of a DNA ssOrigami

Although various DNA nanostructures have been created in a multistranded format, simply breaking and reconnecting strands from existing scaffolded origami designs would not solve a key challenge in designing ssOrigami, which is to create an ssOrigami structure with minimal knotting complexity to avoid being kinetically trapped during the folding process.

To precisely quantify the knotting complexity of different ssOrigami models to facilitate the design process, we can convert an open-chain linear DNA strand into a closed loop by connecting its 5′ and 3′ ends, and then characterize the topological complexity of this closed loop, which can be treated as mathematical knots. Two DNA knots are homotopic if they can be transformed into each other through a continuous deformation, which means that strands cannot be cut during any operation (fig. S3-3) (*55*). Such rules also apply to ssOrigami because the nucleic acid backbone cannot be cut or intersected during the folding process. The knotting complexity of ssOrigami designs can be approximately described by the crossing number, a knot invariant defined as the smallest number of crossings found in any diagram of the knot (*56*, *57*).

If a knot has a crossing number of zero, then it is topologically equivalent to an unknotted circle (also referred as an unknot). In nature, most of the RNA and protein structures have a crossing number of 0, and only in rare cases, some proteins may have very small crossing number (*58*–*61*). On the contrary, as shown in fig. S3-4, ssOrigami designs derived from traditional scaffolded DNA origami structures tend to result in complex knots with high crossing numbers, which will likely hinder proper folding.

To achieve the ssOrigami structures with small crossing number, our first consideration in ssOrigami design is to choose between antiparallel and parallel crossovers for interhelical cohesion. As shown in Fig. 1A, at every antiparallel crossover position, DNA strands need to run through the central plane that contains all the parallel DNA helical axes (dashed lines in the model), like threading a needle through a piece of fabric (see also fig. S3-5). On the contrary, as shown in Fig. 1B, at parallel crossover positions, DNA strands do not go through this plane, which could reduce the knotting complexity of the structure.

We next specify designed parameters based on parallel crossovers. We create an illustrative partially paired double-strand intermediate (Fig. 1, C to E) and further fold this double strand into designed shapes (Fig. 1, F to H). This design has continuous π-π stacking along all the helices and has uninterrupted base-pairing sections that are long enough [≥6 base pairs (bp)] to provide necessary structural stability. Also, this design has simple topology with a crossing number of 0 (see also section S5). In the three-dimensional (3D) models shown in Fig. 1 (C and F), the white and gray cylinders are used to denote uninterrupted base pairs and different domains; whenever there is a nick point in the helices, the cylinder breaks. By separating these cylinders into two groups, we can see that most of the ssOrigami (Fig. 1, C and F) contains two distinct domains: the 10-bp helical domains (white cylinders) and the 6-bp locking domains (gray cylinders), which are also depicted as rectangles and crosses in Fig. 1 (D and G). Each locking domain is between two adjacent parallel crossovers, and all blue strands are on top of red strands at crossover points in this design. One of the key features in this design is that all the blue domains (top layer) are covalently linked in a raster-filling pattern and then connected to the red domains (bottom layer), which have symmetrical geometry.

In Fig. 1 (E and H), to help visualize the folding track of the covalently linked illustrative intermediate structure, we created a pipeline style model and colored it with a rainbow gradient in which the 5′ and 3′ ends of the intermediate are red and the middle of the ssDNA is purple. This intermediate contains paired helical domains and unpaired single-stranded regions. When all the locking domains are further formed through base pair recognition (Fig. 1I), the intermediate will become the fully folded ssOrigami structure. Using this design strategy, we have designed a variety of $m \times n$ rhombus-shaped ssOrigami (Figs. 1H and 3, A to D), where m denotes the number of diagonally oriented, partially paired helices in the top layer and n denotes the number of partially paired helices in the bottom layer. The structure in Fig. 1H is thus referred to as a 5×5 rhombus ssOrigami.

This 5×5 rhombus ssOrigami has a crossing number of 0. Although the DNA strand needs to go through the central plane many times in the design, such plane crossings all happen on the helical domains but not on the locking domains. To illustrate that this ssOrigami design is not knotted, we created a dynamic relaxation system in which the ssOrigami pipeline model is relaxed under simulated gravity while fixing both of its ends (see section S4). Under this relaxation, the ssOrigami becomes an unknotted rope (double-stranded), revealing that it has a crossing number of 0 (shown in Fig. 1J). Such a double-stranded pipeline can be further relaxed under simulated gravity into a single-stranded open loop with its 3′ and 5′ ends fixed, which also has a crossing number of 0 (figs. S3-3D and S4-1A).

Synthesis and characterization of a DNA ssOrigami

Another challenge for constructing ssOrigami stems from the difficulty of synthesizing the ssDNA. Because self-complementarity is an intrinsic property of ssOrigami, its strong secondary structure may present challenges to synthesizing the DNA. As a result, minimization of local self-interaction is a key part of ssOrigami structure design. To decrease self-complementarity, we first limit the length of most helical domains to 10 bp (as in Fig. 1). Then, we further split the ssDNA strand into two approximately equal halves to separate all helical domain sections, which decreases the self-interaction substantially (Fig. 2A). A 30-bp overlap (yellow regions) is added to the ends of two half strands so that they can be joined and amplified at the same time through a one-step polymerase chain reaction (PCR; Fig. 2B). Two different primers are used in the PCR step: primer 1 (green) with a 5′ phosphorothioate modification and primer 2 (orange) with a 5′ phosphorylation modification. Because the phosphorothioate modification

Downloaded from https://www.science.org on November 16, 2023

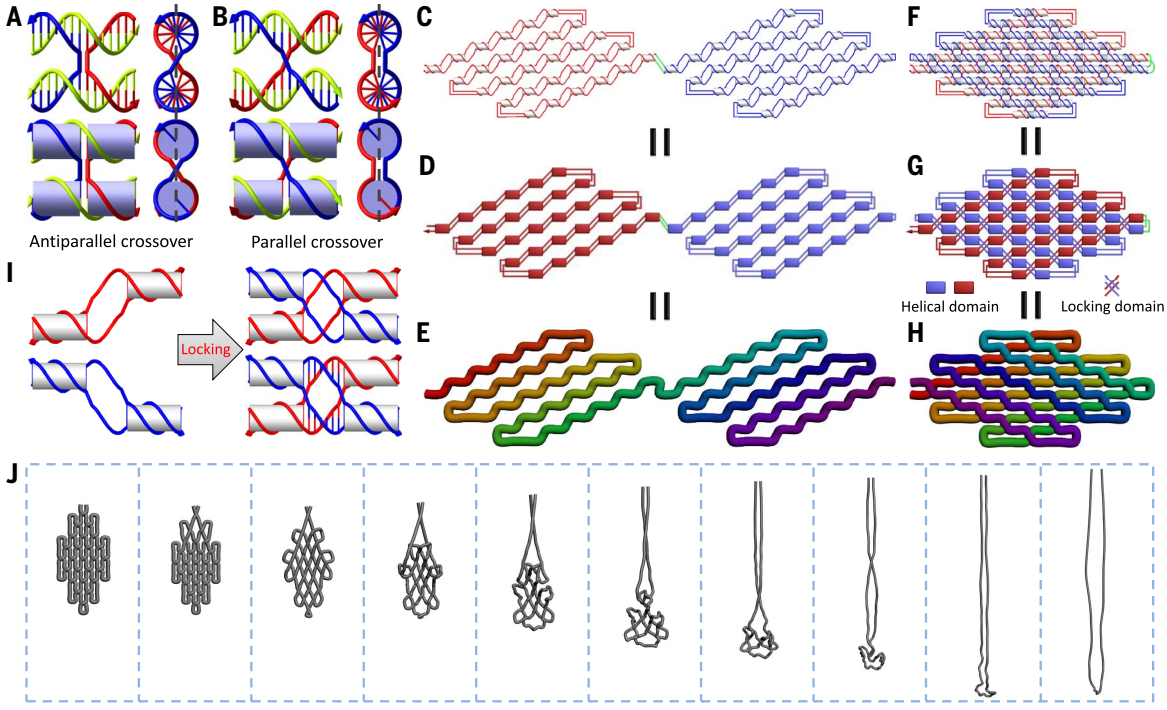


Fig. 1. Design of ssOrigami. (**A** and **B**) Schematics of the antiparallel crossover designs (A) and the parallel crossover designs (B) illustrating their local topology. The dashed lines denote the plane containing all DNA helical axes. (**C** to **E**) Models of a typical illustrative double-stranded intermediate for ssOrigami. (**F** to **H**) Models of a fully formed ssOrigami structure. (C and F) Double helical models with cylinders depicting the uninterrupted base pairs. (D and G) Carton models highlighting the 10-bp helical domains (rectangles) corresponding to the white cylinders in (C) and (F) and 6-bp locking domains (crosses) corresponding to the gray cylinders in (F). Bottom-layer strand sections and rectangles are colored in red, and the top-layer ones are colored in blue, whereas the green lines denote the connection between the red layer and the blue layer in (C), (D), (F), and (G). (E and H) Pipeline style models representing the folding track of the double-stranded intermediate. The model is colored with rainbow gradient starting from the 5′ and 3′ ends (red) to the middle of the strand (purple). (**I**) Schematic depicting the formation of a locking domain. (**J**) Dynamic relaxation model showing a time-lapse snapshot of the relaxation process of an ssOrigami pipeline model (H) under simulated gravity, with both of its ends fixed (see also movie S12; notice that the dynamic relaxation movie does not necessarily reflect the real dynamic folding process of ssOrigami, and it instead serves as an analysis tool to visualize the knotting complexity of the structure).

on the forward strand renders the internucleotide linkage resistant to nuclease degradation, whereas phosphorylation makes the reverse strand a substrate for DNA exonuclease, only the reverse strand will be digested by lambda exonuclease, yielding the protected ssDNA strand (Fig. 2C).

The DNA strand was then folded in 12.5 mM Mg^{2+} buffer (Fig. 2D; see Materials and Methods for details) using a 2-hour annealing ramp from 85° to 25°C. Gel electrophoresis revealed expected product band migration pattern (fig. S6-2C) after PCR (Fig. 2B), exonuclease digestion (Fig. 2C), and folding (Fig. 2D). The folded product was then visualized using atomic force microscopy and exhibited expected rhombus morphology (Fig. 2, K and L).

In vitro and in vivo replication of DNA ssOrigami

Similar to previous ssDNA nanostructures (*3*, *41*–*45*), a key design feature of ssOrigami is that it can be replicated in vitro (*3*, *41*–*43*) and in living cells (*43*, *45*). To test its in vitro replicability, the folded rhombus ssOrigami in Fig. 2D was used as a template for another round of PCR amplification (indicated by the arrow from Fig. 2D to Fig. 2B). Specifically, instead of the two original double-stranded template strands, the previously folded ssOrigami product was added to the PCR mixture to produce the amplified dsDNA product. After repeating the synthesis processes under the same experimental conditions, the ssDNA template was successfully replicated, and the annealed structures were imaged under atomic force microscopy (AFM) (Fig. 2M) and produced identical morphology as the pre-amplified ssOrigami in Fig. 2 (K and L). In control experiments with no polymerase, the ssOrigami was not replicated (fig. S6-3). The above experiment thus shows that PCR can effectively replicate and produce ssDNA origami sequences in vitro.

We next sought to replicate the rhombus ssDNA origami "genes" in vivo (*43*, *45*). The double-stranded gBlock DNA fragments with restriction enzyme sites (Fig. 2E) were ligated into a single-plasmid vector (Fig. 2F). Such ligation products were later transformed into *Escherichia coli* cells, and the plasmids containing ssOrigami genes were thus amplified in vivo as the bacteria population grows (Fig. 2, G and H). The amplified plasmids were purified and treated by the nicking endonuclease Nb.BbvCI and the restriction endonuclease Hind III (Fig. 2I). As a result, the plasmid DNA was separated into three single-stranded pieces, and the target ssDNA was then extracted by denaturing agarose gel electrophoresis (Fig. 2J; see fig. S7-2 for denaturing gel electrophoresis results). The ssDNA was then folded into the target structure, and native gel electrophoresis confirmed the expected migration pattern for the pre- and post-folding strand, and revealed high folding yield (~95%; see figs. S7-3 and S7-4 for native gel results and yield quantification details). AFM imaging revealed expected morphology (Fig. 2N).

In addition to the 5 × 5 rhombus ssOrigami (containing 2238 nt), two more ssOrigami structures (a 5 × 10 rhombus ssOrigami with 3940 nt in Fig. 3C and a triangle frame–shaped ssOrigami with 3439 nt in Fig. 3H) were successfully cloned and replicated in living cells and produced strands that fold with high yields (~90%; see figs. S7-3 and S7-4 for details), confirming the generality of the clonability of ssOrigami.

Because plasmid DNA can be easily replicated in *E. coli*, the production can be scaled up by growing a large volume of *E. coli* cells with low cost. Another advantage of cloning is high DNA replication fidelity because *E. coli* cells have various machineries for DNA replication, such

Downloaded from https://www.science.org on November 16, 2023

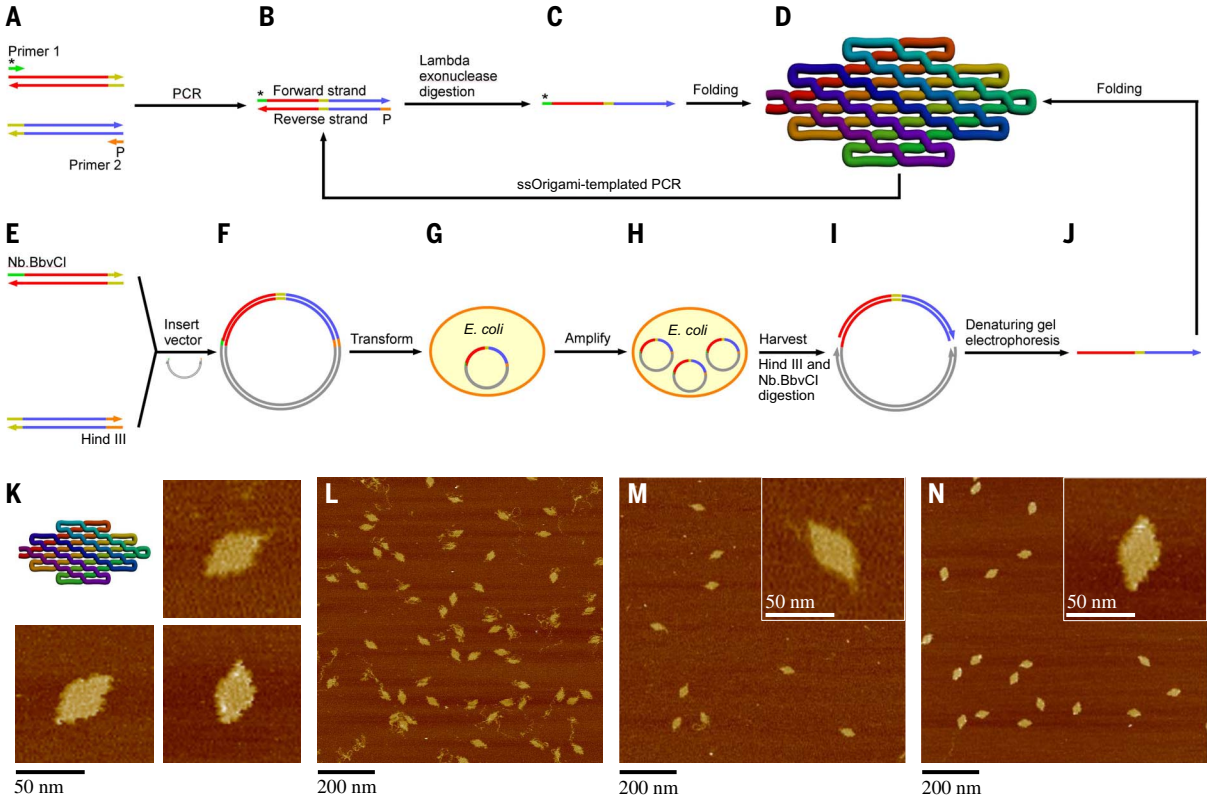


Fig. 2. Schematic of ssOrigami synthesis and replication by in vitro PCR and by in vivo cloning of ssOrigami genes. (**A**) One-step PCR with two double-stranded gBlock templates containing 30-bp sequence overlap (yellow sections) and two modified primers (phosphorothioate modification on green primer and phosphorylation modification on red primer). (**B**) Double-stranded PCR product with modified 5′ ends. (**C**) ssDNA product after lambda exonuclease digestion. Phosphorothioate modification protects the forward strand from being digested. (**D**) Folded ssOrigami structure. Note that the folded ssOrigami product can be directly used as a template for its PCR replication. (**E**) Double-stranded gBlock DNA fragments with restriction enzyme sites designed at both ends. (**F**) Ligation of two half fragments into linearized pGEM-7zf (−) vector to form the full-length ssOrigami gene. (**G**) The ligation products were transformed into *E. coli* NEB stable competent cells. (**H**) Full-length ssOrigami genes were amplified as plasmid DNA in *E. coli* NEB stable cells. (**I**) The harvested genes were treated by the nicking endonuclease Nb.BbvCI and the restriction endonuclease Hind III. (**J**) The double-digestion products were denatured using 8 M urea, and the target ssDNA was separated from a denaturing agarose gel (see also fig. S7-2). (**K** and **L**) Schematic (K) and AFM images [(K), zoomed-in; (L), large field of view] of the 5 × 5 ssOrigami structures produced by the PCR synthesis [first cycle in (A) to (D)]. (**M**) AFM image of 5 × 5 ssOrigami structures produced by PCR replication method [the second cycle in (A) to (D), that is, the re-PCR product]. (**N**) AFM image of 5 × 5 rhombus ssOrigami produced by in vivo cloning method. Detailed experimental information is shown in sections S6 (in vitro PCR) and S7 (in vivo cloning).

as DNA repair systems. The mutation rate of the *E. coli* DNA replication machinery is only ~10^{-10}, which is four orders of magnitude lower than the highest-fidelity PCR polymerase (*62*).

Scalability and shape versatility of DNA ssOrigami

To test the scalability of the ssOrigami design, in addition to the 2238 nt 5 × 5 rhombus structure, we constructed a series of 3 × 3, 4 × 4, 5 × 10, and 12 × 12 rhombus shapes containing 966, 1538, 3940, and 10,682 nt, respectively (Fig. 3, A to D, top), and observed expected morphologies under AFM (Fig. 3, A to D, middle and bottom). In the software tool section, a 3116-nt 6 × 6 rhombus (Fig. 6L) was also demonstrated. The successful formation of these distinct-sized rhombus structures demonstrates the ease for scaling (both up and down) the ssOrigami design. The 10,682-nt rhombus ssOrigami is 37 times larger than the previous largest ssDNA structure (*43*) and 16 times larger than the previous largest ssRNA structure (*44*) and approaches the complexity of scaffolded DNA origami (*4*).

To test the shape versatility of ssOrigami design, in addition to rhombus shapes, a 2849-nt heart shape (Fig. 3E), two horizontal heart shapes (1338 and 2032 nt; Fig. 6, M and N), a 2166-nt rectangle (Fig. 3F), a 1884-nt rectangle (Fig. 3G), a 3873-nt disc shape (Fig. 4A), and a 3898-nt square shape (Fig. 4C) were constructed. In addition, we created a 3439-nt triangle frame-shaped ssOrigami from three rectangle subunits (Fig. 3H). The strands for the structures were PCR-synthesized as in the previous section, folded in 12.5 mM Mg^{2+} buffer using a 2- to 12-hour annealing ramp from 85° to 25°C, and visualized using AFM with expected morphology. Together, 18 distinct ssOrigami shapes were constructed, suggesting the shape generality of the ssOrigami design.

Besides different sizes and shapes, the ssOrigami design can also accommodate different routing strategies. In the rectangle and square ssOrigami structures (Figs. 3, F and G, and 4C), the double-stranded pipe is designed to wrap along the helical direction several times instead of raster-filling the bottom and top layers. Another difference between rectangle-shaped ssOrigami and rhombus-shaped ssOrigami is that the rectangular design contains several 26-bp helical domains on its long edges (figs. S5-5 and S5-6), which bridge the bottom- and top-layer strands. Despite their diverse size, geometry, and routing, the crossing numbers for all the 18 ssOrigami structures remain 0, as verified by the dynamic relaxation process (Fig. 1J and figs. S5-8 to S5-12).

Programmable patterning on ssOrigami

In addition to programmable shapes, ssOrigami can produce programmable surface patterns. Similar to previous multistranded scaffolded DNA origami (*4*, *8*) and DNA brick (*14*, *15*) structures, ssOrigami generates space-filling structures. An

Downloaded from https://www.science.org on November 16, 2023

important consequence of the space-filling nature of the structure is that it provides a platform for arranging surface features and scaffolding external molecular cargoes in arbitrary, user-prescribed spatial patterns.

Figure 4A describes the design schematic for arranging dumbbell-shaped hairpins (*4*) at 10 user-prescribed positions on a disc-shaped ssOrigami surface to mimic a smiley face pattern. The hairpins are fully integrated into the disc structure without increasing its crossing number: Despite its complex geometry, the entire structure remains as an unknotted single strand. Under AFM, these hairpins were visualized as raised surface protrusions at the designed locations (Fig. 4B).

Figure 4C describes the design schematic for a 3898-nt square-shaped ssOrigami that displays four 45-nt single-stranded loops. These loops can serve as "handle" to scaffold other functional molecules attached to complementary anti-handle DNA strands. In Fig. 4E, biotinylated DNA anti-handles are introduced and followed by incubation with streptavidin, which binds to biotin.

AFM images in Fig. 4D reveal the expected square morphology of structure. In contrast to the double-stranded dumbbell hairpins in Fig. 4B, the single-stranded loops are not as visible. After the introduction of streptavidin, four white protrusions can be spotted (Fig. 4F), consistent with the attachment of streptavidin at the four designated positions.

Design and synthesis of RNA ssOrigami

Strikingly, the DNA ssOrigami design strategy can be adapted to create RNA ssOrigami by merely changing the helical and/or locking domain lengths to account for the helical periodicity difference between the 10.5 bp/turn for DNA's B-type helix and the 11 bp/turn for RNA's A-type helix. In the DNA ssOrigami design, the helical domain and the locking domain are 10 and 6 nt, respectively, in length. Hence, every 32 bp contains two 10-nt helical domains interspersed with two 6-nt locking domains. This corresponds to about three full helical turns at 10.67 bp/turn (which slightly deviates from the typical 10.5 bp/turn). We denote this design as 10-6-10-6 design (Fig. 5A). One simple strategy to adapt the DNA design to RNA is to simply change the 10-6-10-6 design to 10-6-11-6 design (Fig. 5B) by increasing the length of the second helical domain by 1 nt. In this design, each structural repeating unit is 33 bp, which corresponds to exactly three full 11-bp RNA A-type helical turns. An alternative design of 8-8-9-8 also gives three turns per 33-bp repeating unit (Fig. 5C).

To synthesize long ssRNA molecules, the DNA template with both T7 and T3 promoter sequences was first synthesized as two fragments similar to the DNA ssOrigami design. The two DNA fragments were subcloned into the same vector through Eco RI and Hind III restriction sites and amplified in *E. coli*. The purified plasmids were then linearized by Eco RI and Hind III, and transcribed using T7 RNA polymerase and/or T3 RNA polymerase (see Fig. 5D, which depicts both). The in vitro transcribed RNA molecules were then purified, self-folded with the same annealing program as DNA ssOrigami, and characterized with AFM.

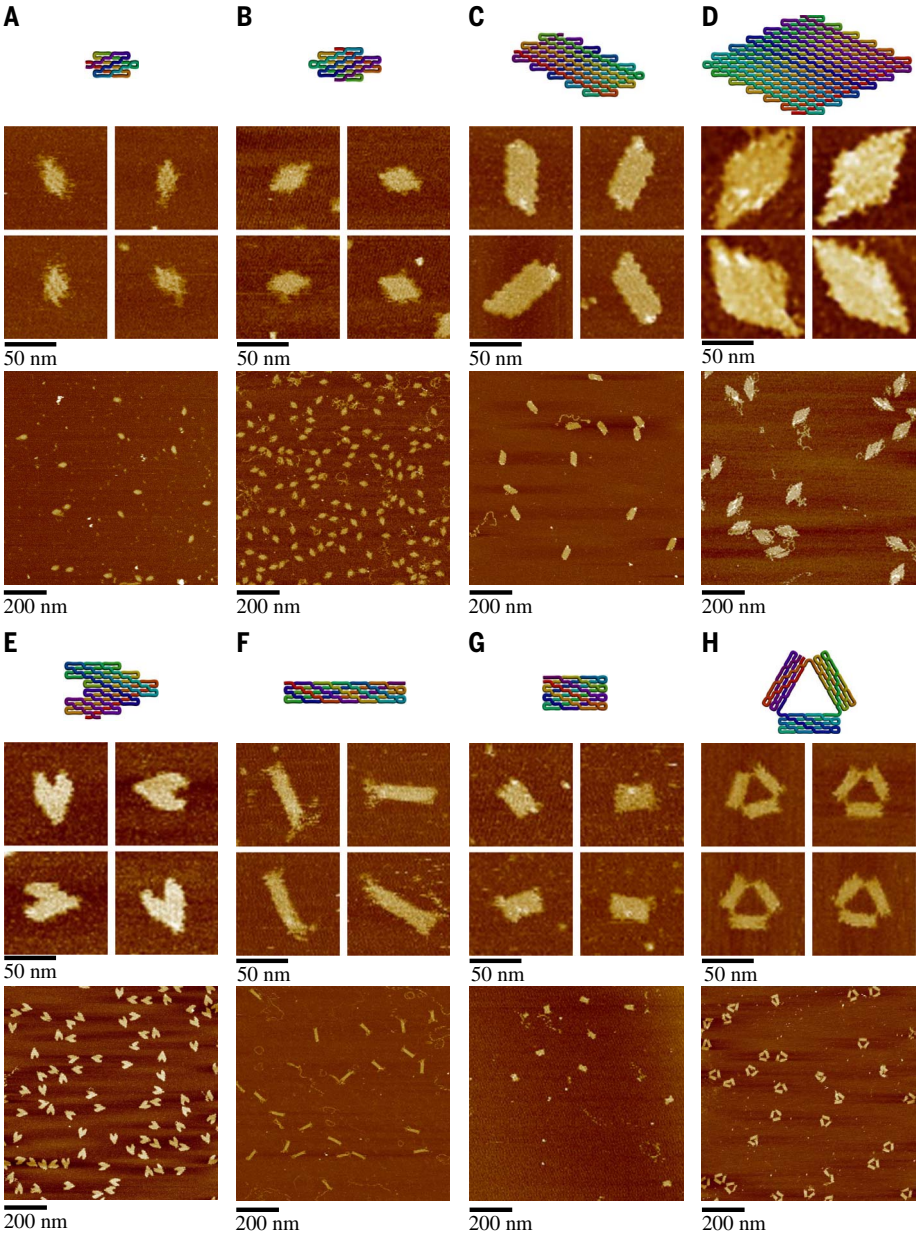


Fig. 3. DNA ssOrigami structures. (**A**) 3 × 3 ssOrigami containing 966 nt. (**B**) 4 × 4 ssOrigami containing 1538 nt. (**C**) 5 × 10 ssOrigami containing 3940 nt. (**D**) 12 × 12 ssOrigami containing 10,682 nt. (**E**) Heart-shaped ssOrigami containing 2849 nt. (**F**) Rectangle-shaped ssOrigami containing 2166 nt. (**G**) Rectangle-shaped ssOrigami containing 1884 nt. (**H**) Triangle-shaped ssOrigami containing 3439 nt. Top row in each panel shows schematic, and middle and bottom rows show zoomed-in and large field-of-view AFM images. See section S11 for additional AFM images.

Using the 10-6-11-6 design, we successfully constructed a 2058-nt rectangle (Fig. 5E) and a 3042-nt heart (Fig. 5F) ssRNA origami. Using the 8-8-9-8 design, we constructed a 1868-nt rectangle (Fig. 5, G and H) and a 6337-nt 9 × 9 rhombus (Fig. 5I) RNA ssOrigami. We tested to transcribe the RNA strand for 1868-nt rectangle from both the sense strand (Fig. 5G) and the antisense strand (Fig. 5H), and both produced expected and identical shapes under AFM. The 6337-nt rhombus RNA ssOrigami is 10 times larger than any previous synthetic discrete RNA nanostructure (*44*).

Automated design software tool

To facilitate the design, we developed a design algorithm and an automated design software tool, which takes as input an arbitrary space-filling shape, and outputs the sequence for a strand that will fold

Downloaded from https://www.science.org on November 16, 2023

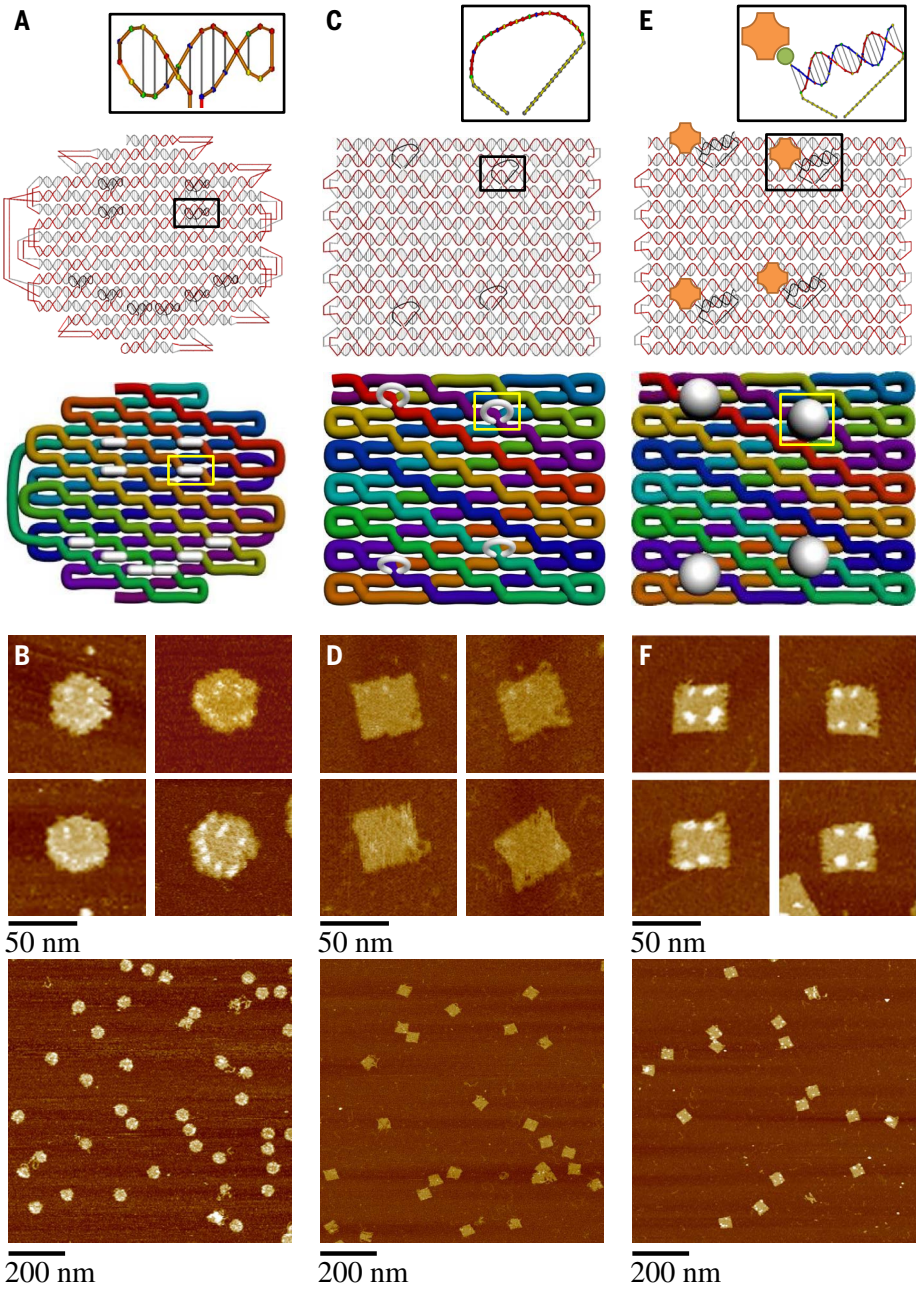


Fig. 4. Programmable patterns of surface features and cargoes on DNA ssOrigami. (**A**) Design schematic of a 3873-nt disc-shaped ssOrigami with hairpin protrusions that mimic the pattern of a smiley face. The top shows the strand diagram, and the inset shows details of the dumbbell hairpin. The bottom is the pipeline schematic where the white line segment represents the hairpin. (**C**) Design schematic for a 3898-nt square-shaped ssOrigami with four single-stranded loops (top inset). (**E**) Design schematic for attaching complementary anti-handles to the loop handles. An anti-handle is modified with a biotin (green dot), which binds to a streptavidin (colored orange in the top panel and represented as white balls in the bottom panel). (**B**, **D**, and **F**) Corresponding AFM images for designs in (A), (C), and (E). See section S11 for additional AFM images.

into a knot-free DNA or RNA ssOrigami that approximates the target shape. Figure 6 (A to H) depicts the workflow for the design algorithm. (i) A target shape (Fig. 6A) is converted into pixelated representation (Fig. 6B). (ii) The pixels are converted into helical domains and locking domains (Fig. 6, C and D). (iii) All the open linear strands are converted into closed cycles by closing each end of each open helix with a hairpin (Fig. 6E). (iv) The cycles on the top layer are merged into one single cycle, and the cycles on the bottom layer are merged into another single cycle (Fig. 6F). (v) The top-layer cycle and the bottom-layer cycle are merged into one single cycle (Fig. 6G). (vi) The sequence is assigned to the cycle strand, and the expected folded structure is visualized (Fig. 6H).

We implemented this design algorithm to create an automated design software tool with a web-based user interface (http://dna.kwonan.com/). The user can upload a 2D image or draw a shape using a 2D pixel design editor. The user can optionally add hairpins or loops, which can serve as surface markers or handles for attaching external entities. The software will then generate ssOrigami structures and sequences, and the user can view the molecular structure via an embedded molecular viewer (*63*). The user can also export the molecular structure and the DNA sequence in various file formats (.pdb, .cif, .dnajson, .bas, and .csv) for analysis with other simulation or analysis toolkits, and the ssOrigami can be further inspected, analyzed, and, if necessary, modified. Finally, the DNA sequences will be synthesized and folded into target structures. Figure 6 (I to N) shows six examples of DNA ssOrigami structures, which were designed using the software tool, synthesized, folded, and characterized under AFM.

Discussion

We have constructed ssOrigami structures from both ssDNA and ssRNA with synthetic sequences ranging in length from ~1000 to ~10,000 nt, which represents the largest unimolecular folding of a synthetic nucleic acid structure that has been achieved to date. Compared to the wire-frame DNA octahedron assembled from a 1669-nt scaffold strand and five auxiliary short strands reported in 2004 (*3*), our ssOrigami uses no auxiliary strands and can be designed to form a wide variety of space-filling compact shapes. Meanwhile, compared to the ssRNA nanostructures reported in 2014 (*44*), our design strategies can be applied to both DNA ssOrigami and RNA ssOrigami because it is not limited by RNA kissing-loop interactions (*64*). As a consequence, ssOrigami is a purely de novo designed structure that does not rely on the availability of highly sequence-specific, naturally occurring molecular interaction motifs with defined geometrical arrangements (for example, the RNA kissing loops) and thus promises, in principle, better designability and scalability, as reflected in practice by our construction of a 10,682-nt ssDNA structure and 6337-nt ssRNA structure.

Previous work demonstrates the self-assembly of complex structures from hundreds of distinct components (with and without the assistance of a scaffold), and the ssOrigami work here demonstrates the folding of complex structures from a single strand. Therefore, previous multicomponent assembly work (scaffolded origami and DNA bricks) and the current unimolecular folding work represent two extremes for engineering synthetic nucleic acid nanostructures, and together promise a vast design space in between. In an attempt to probe this space, we separated the 2238-nt ssOrigami strand (Fig. 2C) into two 1119-nt strands or twenty ~90-nt strands (each spanning the

Downloaded from https://www.science.org on November 16, 2023

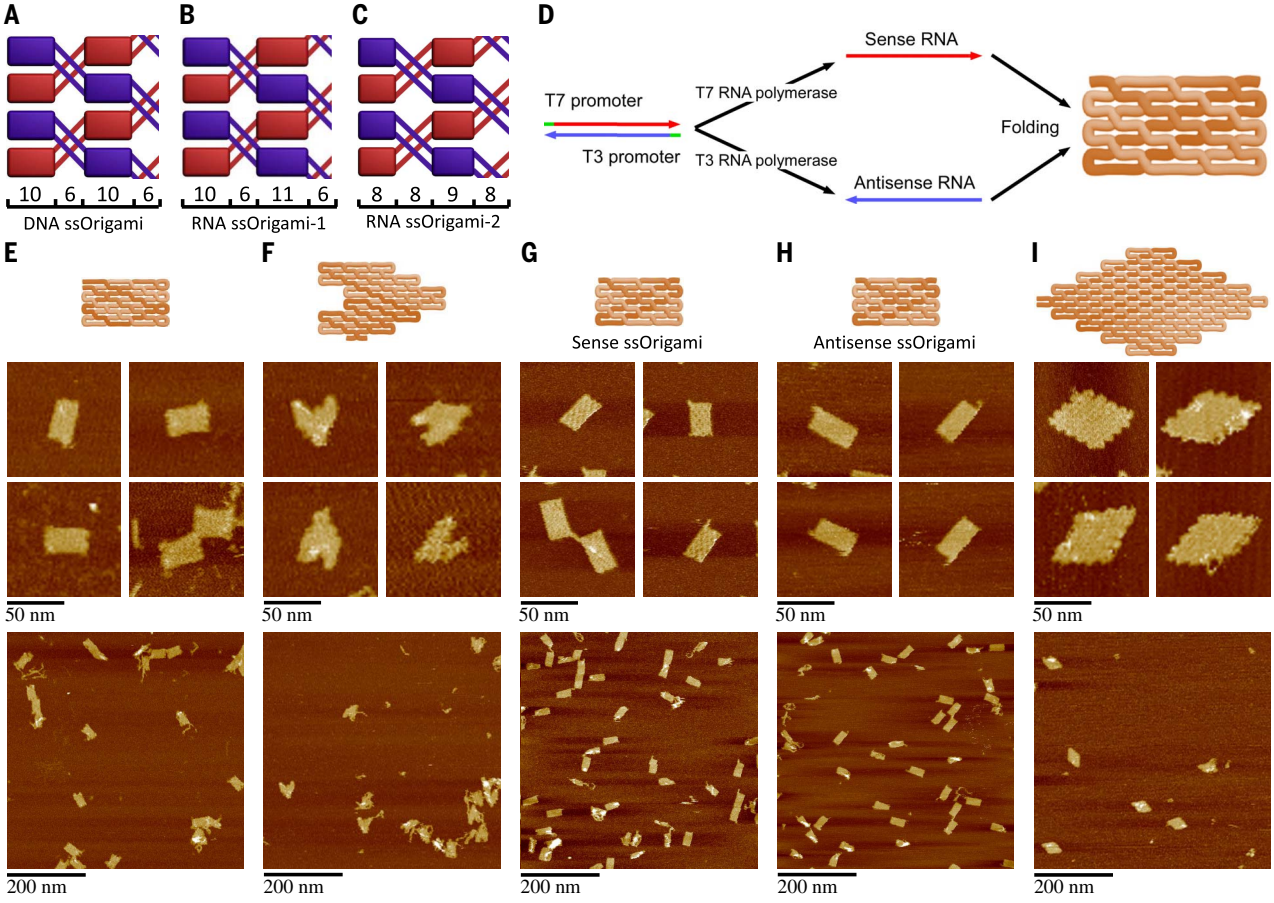


Fig. 5. RNA ssOrigami. (**A** to **C**) Design schematics for 10-6-10-6 DNA ssOrigami design (A), 10-6-11-6 RNA ssOrigami design (B), and 8-8-9-8 RNA ssOrigami design (C). Similar to Fig. 1G, helical domains and locking domains are represented as rectangles and crosses. The bottom axis shows the length of each domain. (**D**) Schematic showing the synthesis of both sense and antisense RNA ssOrigami structures. (**E** and **F**) Schematics (top) and AFM images (bottom) of a 2058-nt rectangle-shaped (E) and a 3042-nt heart-shaped (F) RNA ssOrigami using the 10-6-11-6 design depicted in (B). (**G** to **I**) Schematics (top) and AFM images (bottom) of a 1868-nt rectangle-shaped (G and H) and a 6337-nt 9 × 9 rhombus-shaped (I) RNA ssOrigami using the 8-8-9-8 design in (C). Both the sense strand (G) and antisense strand (H) rectangle ssOrigami are constructed following the workflow depicted in (D).

diameter of the shape); both cases successfully assembled into the same target shape as in the unimolecular folding case (see section S10), further suggesting the presence of such a rich design space awaiting further exploration (*65*).

Materials and methods

Materials

Double-stranded DNA (dsDNA) templates were purchased from Integrated DNA Technologies Inc. as gBlocks at 200-ng synthesis scale. Primers including 5′ phosphorothioate modification (T*T*T*T*T*T*) or 5′ phosphorylation (/5Phos/) were purchased from Integrated DNA Technologies Inc. at 100-nmol synthesis scale with HPLC purification. Phusion High-Fidelity PCR Master Mix with HF Buffer (100 reactions/50-liter volume) and Lambda Exonuclease (1000 units) was purchased from New England Biolabs, Inc. MinElute PCR Purification Kit was purchased from QIAGEN. Nicking endonuclease Nb.BbvCI (1000 units), restriction endonucleases Eco RI (5000 units), Xho I (5000 units) and Hind III (5000 units), T7 and T3 RNA polymerases (5000 units), PCR Cloning Kit (20 reactions), NEB 10-beta and NEB stable competent *E. coli* were purchased from New England Biolabs, Inc. pGEM-7zf (–) vector, Pureyield plasmid miniprep system, and the Wizard SV Gel and PCR Clean-UP System were purchased from Promega. RNA Clean and Concentrator-25 was purchased from Zymo Research.

DNA and RNA sequence design

DNA ssOrigami sequences were designed with the Tiamat software (*66*). Sequence generation of ssOrigami structures uses the following criteria in the software: (1) Unique sequence limit: 8–10; (2) repetition limit: 8; (3) G repetition limit: 4; (4) G/C percentage: 0.38–0.5. The RNA ssOrigami sequences were also designed with the Tiamat software, with the same sequence generation criteria as for the DNA ssOrigami. After the DNA template sequences were generated, the T7 and T3 promoter sequences followed with two or three consecutive Gs were added to the ends to facilitate efficient in vitro transcription reactions.

Dynamic relaxation model

Our dynamic relaxation model is realized by the Autodesk 3ds Max software. Spline models of target structure are first created and treated as a fix-ended soft rope. Such rope is relaxed under simulated gravity at the chosen direction. Details about this model such as the animation parameters and the falling direction set up are described in section S4.

In vitro PCR sample preparation

ssDNA was synthesized by multitemplate polymerase chain reaction followed by Lambda Exonuclease treatment. A typical PCR reaction solution contained 25 μl 2× Phusion High-Fidelity PCR Master Mix with HF Buffer, 23 μl 8% DMSO, 0.5 μl gBlock DNA (4 ng/μl) for both templates, 0.5 μl phosphorothioate primer (forward, 100 μM) and 0.5 μl phosphate primer (reverse, 100 μM).

Downloaded from https://www.science.org on November 16, 2023

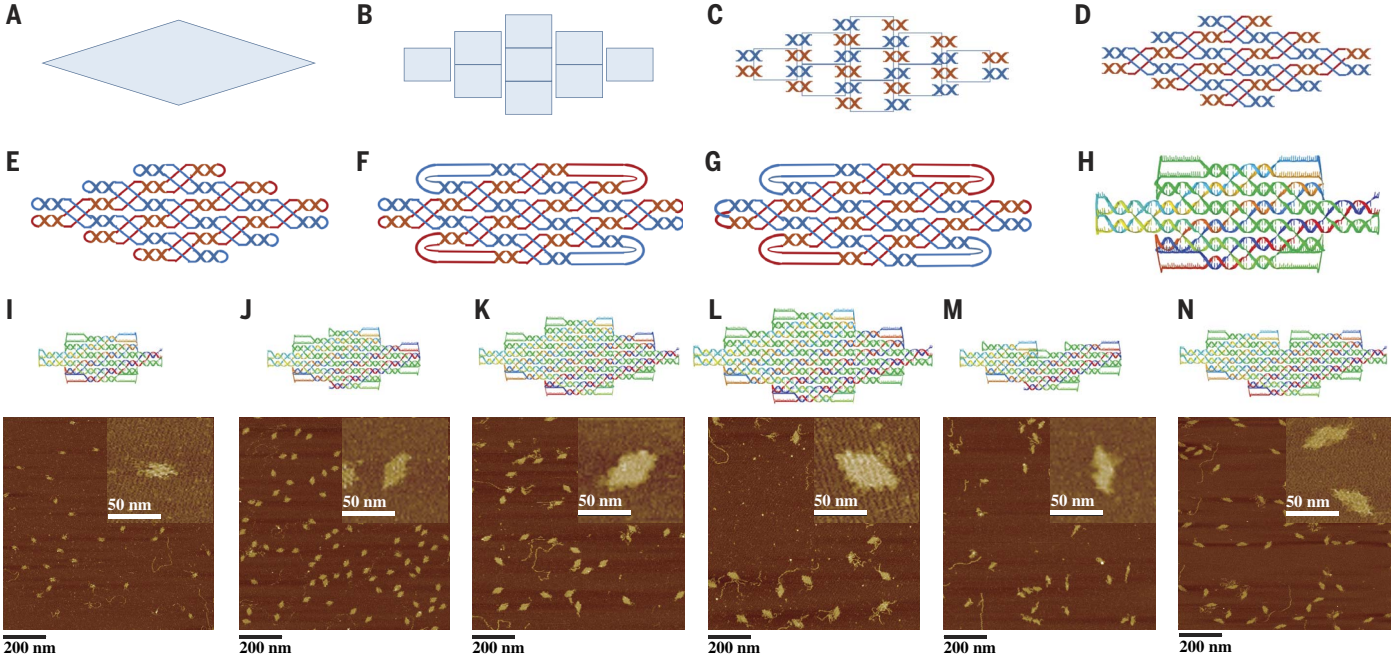


Fig. 6. Workflow and validation of automated design software. (**A** to **H**) Design algorithm workflow. (A) Input shape. (B) Pixelated shape. (C) Four helical domains assigned to each pixel. (D) Two locking domains assigned to each pixel to connect helical domains. (E) Hairpins added to the ends of helices, converting all strands to closed cycles. Top and bottom layer cycles are respectively colored in blue and red. (F) All top blue cycles are merged into one single cycle; all bottom red cycles are merged into one cycle. (G) Top blue cycle and bottom red cycle are connected at the left end and merged into one cycle. (H) Sequences assigned to the cycle (not depicted) and the final ssOrigami shape visualized. (**I** to **N**) Strand diagrams rendered by the software (top) and AFM images (bottom) for six DNA ssOrigami shapes: a 1016-nt 3 × 3 rhombus (I), a 1588-nt 4 × 4 rhombus (J), a 2238-nt 5 × 5 rhombus (K), a 3116-nt 6 × 6 rhombus (L), a 1338-nt heart (M), and a 2032-nt heart (N) shape.

Primers were designed to have melting temperatures of 64°C to minimize the impact of the secondary structure of the DNA template. A typical PCR reaction was as follows: (1) Initial denaturation at 98°C for 30 s; (2) 25 to 35 cycles of 10 s at 98°C (strand separation stage), 30 s at 65°C (annealing stage), and 1 min at 72°C (polymerase extension stage); (3) final extension for 10 min at 72°C; (4) hold at 4°C after reaction.

After PCR, 50 μl of PCR product was purified using the QIAGEN MinElute PCR Purification Kit according to the manufacturer's instructions. A volume of 100 μl H_2O was used for elution of DNA after the spin columns purification. The purified DNA was then treated with Lambda Exonuclease. Typically, 5 μl 10× Lambda Exonuclease buffer and 5 μl Lambda Exonuclease (5000 units/ml) were added to 40 μl of dsDNA solution for reaction. The mixture was incubated for 12 hours at 37°C, and then boiled at 98°C for 5 min to inactivate the enzyme before use. The product (ssDNA) was either directly added to a folding reaction or gel-purified using Squeeze 'N Freeze columns (Bio-Rad) before adding to 1× TAE Mg^{2+} buffer (40 mM Tris, 20 mM acetic acid, 2 mM EDTA, and 12.5 mM magnesium acetate, pH 8.0) for folding. The resulting solution was annealed from 85° to 25°C to form the designed structures. The steps for the slow annealing were as follows: 85° to 60°C at 1°C per 10 min; 60° to 40°C at 1°C per 30 min; 40° to 25°C at 1°C per 15 min. The steps for the fast annealing were as follows: 85° to 65°C at 1°C per 1 min; 65° to 45°C at 1°C per 5 min; 45° to 25°C at 1°C per 1 min. All samples were then subjected to AFM imaging without further purification.

In vivo cloning sample preparation

ssDNA origami designs were divided into two DNA sequences with restriction sites designed on both sides and ordered from IDT as gBlocks fragments. In the case of 2238-nt 5 × 5 ssOrigami structure, the first fragment had Eco RI and Xho I sites, whereas the second fragment had Xho I and Hind III sites. The Nb.BbvCI site was designed next to Eco RI site on the first fragment for the purpose of nick generation in the final step. The two gBlock fragments (blunt-ended) were individually ligated with pMiniT vector (blunt-end vector from NEB PCR cloning kit) following the manufacturer's instruction. The ligation products were transformed into *E. coli* NEB-10beta competent cells (included in the PCR cloning kit). *E. coli* colonies were formed after overnight growth, and single colonies were picked up for overnight growth in LB medium. Plasmid minipreps were performed from overnight *E. coli* cultures. The plasmids with inserts were sent for DNA sequencing to screen for error-free clones. The mutation-free plasmids were digested by restriction enzymes accordingly (Eco RI and Xho I for fragment 1 plasmid, and Xho I and Hind III for fragment 2 plasmid). In the next step, the two digested fragments were ligated with Eco RI and Hind III digested pGEM-7zf (–) vector, and transformed into *E. coli* cells (NEB stable competent cells). This was a three-fragment ligation to form a circular piece of DNA. The vector Eco RI sticky end was ligated with the fragment 1 Eco RI sticky end; the fragment 1 Xho I sticky end was ligated with the fragment 2 Xho I sticky end; and the fragment 2 Hind III sticky end was ligated with the vector Hind III sticky end. After the same cloning steps (fig. S7-1h-j), single colonies were picked the next day, and plasmids were purified. Hind III and Nb.BbvCI double digestion were then carried out. The digested products were heated at 90°C for 10 min in denaturing buffer (10 mM Tris–HCl, pH 8.0, 1 mM EDTA and 8 M urea) and loaded onto a 1% urea denaturing agarose gel (in 1× TAE with 1 M urea). After extraction, the ssDNA was annealed using slow or fast annealing programs and imaged with AFM. ssRNA origami samples were prepared similarly. The DNA templates for transcribing ssRNAs were divided into two DNA sequences with both T7 and T3 promoter sequences added to the ends, and ordered as gene synthesis products from Bio Basic Inc. The two fragments were then subcloned into pUC19 vector using the same restriction sites as for ssDNA origami. The final plasmids were linearized by Eco RI and Hind III, and transcribed by T7 or T3 RNA polymerase following the manufacturer's instruction (New England Biolabs). The

Downloaded from https://www.science.org on November 16, 2023

transcription reaction mixture was purified by RNA Clean and Concentrator kit as described in the manufacturer's instruction (Zymo Research). After purification, the ssRNA was annealed using the same program as ssDNA origami.

AFM imaging

For AFM imaging, the sample (15 µl) was deposited onto a freshly cleaved mica surface (Ted Pella, Inc.) and left to adsorb for 1 min. A volume of 40 µl of 1× TAE-Mg^{2+} and 2 to 15 µl 100 mM $NiCl_2$ was added onto the mica, and the sample was scanned on a Veeco 5 Multimode AFM in the Scanasyst in Fluid mode using scanasyst in fluid+ tips (Veeco, Inc.).

Yield quantification with native agarose gel electrophoresis

Yields of ssOrigami structures were estimated by analysis using native agarose gel electrophoresis. The ratio between the fluorescence intensity of the target band and that of the entire lane was used to represent the gross yield of structure formation while background intensity was subtracted from the measured intensity for correction. See figs. S7-3 and S7-4 for details. Please note, as native gel electrophoresis cannot separate DNA Origami structures (including ssOrigami structures) with minor defects, such yield estimation will usually be higher than the real yield. AFM yield is also calculated and compared with gel yield in the supplementary sections.

REFERENCES AND NOTES

1. J. Chen, N. C. Seeman, Synthesis from DNA of a molecule with the connectivity of a cube. *Nature* **350**, 631–633 (1991). doi: 10.1038/350631a0; pmid: 2017259
2. E. Winfree, F. Liu, L. Wenzler, N. Seeman, Design and self-assembly of two-dimensional DNA crystals. *Nature* **394**, 539–544 (1998). doi: 10.1038/28998; pmid: 9707114
3. W. Shih, J. Quispe, G. Joyce, A 1.7-kilobase single-stranded DNA that folds into a nanoscale octahedron. *Nature* **427**, 618–621 (2004). doi: 10.1038/nature02307; pmid: 14961116
4. P. Rothemund, Folding DNA to create nanoscale shapes and patterns. *Nature* **440**, 297–302 (2006). doi: 10.1038/nature04586; pmid: 16541064
5. Y. He *et al*., Hierarchical self-assembly of DNA into symmetric supramolecular polyhedra. *Nature* **452**, 198–201 (2008). doi: 10.1038/nature06597; pmid: 18337818
6. J. Zheng *et al*., From molecular to macroscopic via the rational design of a self-assembled 3D DNA crystal. *Nature* **461**, 74–77 (2009). doi: 10.1038/nature08274; pmid: 19727196
7. H. Gu, J. Chao, S.-J. Xiao, N. C. Seeman, Dynamic patterning programmed by DNA tiles captured on a DNA origami substrate. *Nat. Nanotechnol.* **4**, 245–248 (2009). doi: 10.1038/nnano.2009.5; pmid: 19350035
8. S. M. Douglas *et al*., Self-assembly of DNA into nanoscale three-dimensional shapes. *Nature* **459**, 414–418 (2009). doi: 10.1038/nature08016; pmid: 19458720
9. H. Dietz, S. M. Douglas, W. M. Shih, Folding DNA into twisted and curved nanoscale shapes. *Science* **325**, 725–730 (2009). doi: 10.1126/science.1174251; pmid: 19661424
10. E. S. Andersen *et al*., Self-assembly of a nanoscale DNA box with a controllable lid. *Nature* **459**, 73–76 (2009). doi: 10.1038/nature07971; pmid: 19424153
11. A. Rajendran, M. Endo, Y. Katsuda, K. Hidaka, H. Sugiyama, Programmed two-dimensional self-assembly of multiple DNA origami jigsaw pieces. *ACS Nano* **5**, 665–671 (2011). doi: 10.1021/nn1031627; pmid: 21188996
12. S. Woo, P. W. K. Rothemund, Programmable molecular recognition based on the geometry of DNA nanostructures. *Nat. Chem.* **3**, 620–627 (2011). doi: 10.1038/nchem.1070; pmid: 21778982
13. D. Han *et al*., DNA origami with complex curvatures in three-dimensional space. *Science* **332**, 342–346 (2011). doi: 10.1126/science.1202998; pmid: 21493857
14. B. Wei, M. Dai, P. Yin, Complex shapes self-assembled from single-stranded DNA tiles. *Nature* **485**, 623–626 (2012). doi: 10.1038/nature11075; pmid: 22660323
15. Y. Ke, L. L. Ong, W. M. Shih, P. Yin, Three-dimensional structures self-assembled from DNA bricks. *Science* **338**, 1177–1183 (2012). doi: 10.1126/science.1227268; pmid: 23197527
16. D. Han *et al*., DNA gridiron nanostructures based on four-arm junctions. *Science* **339**, 1412–1415 (2013). doi: 10.1126/science.1232252; pmid: 23520107
17. R. Iinuma *et al*., Polyhedra self-assembled from DNA tripods and characterized with 3D DNA-PAINT. *Science* **344**, 65–69 (2014). doi: 10.1126/science.1250944; pmid: 24625926
18. Y. Ke *et al*., DNA brick crystals with prescribed depths. *Nat. Chem.* **6**, 994–1002 (2014). doi: 10.1038/nchem.2083; pmid: 25343605
19. K. E. Dunn *et al*., Guiding the folding pathway of DNA origami. *Nature* **525**, 82–86 (2015). doi: 10.1038/nature14860; pmid: 26287459
20. T. Gerling, K. Wagenbauer, A. Neuner, H. Dietz, Dynamic DNA devices and assemblies formed by shape-complementary, non–base pairing 3D components. *Science* **347**, 1446–1452 (2015). doi: 10.1126/science.aaa5372; pmid: 25814577
21. E. Benson *et al*., DNA rendering of polyhedral meshes at the nanoscale. *Nature* **523**, 441–444 (2015). doi: 10.1038/nature14586; pmid: 26201596
22. F. Zhang *et al*., Complex wireframe DNA origami nanostructures with multi-arm junction vertices. *Nat. Nanotechnol.* **10**, 779–784 (2015). doi: 10.1038/nnano.2015.162; pmid: 26192207
23. R. Veneziano *et al*., Designer nanoscale DNA assemblies programmed from the top down. *Science* **352**, 1534 (2016). doi: 10.1126/science.aaf4388; pmid: 27229143
24. N. Avakyan *et al*., Reprogramming the assembly of unmodified DNA with a small molecule. *Nat. Chem.* **8**, 368–376 (2016). doi: 10.1038/nchem.2451; pmid: 27001733
25. D. Liu, G. Chen, U. Akhter, T. Cronin, Y. Weizmann, Creating complex molecular topologies by configuring DNA four-way junctions. *Nat. Chem.* **8**, 907–914 (2016). doi: 10.1038/nchem.2564; pmid: 27657865
26. G. Tikhomirov, P. Peterson, L. Qian, Programmable disorder in random DNA tilings. *Nat. Nanotechnol.* **12**, 251–259 (2017). doi: 10.1038/nnano.2016.256; pmid: 27893729
27. S. L. Sparvath, C. W. Geary, E. S. Andersen, Computer-aided design of RNA origami structures. *Methods Mol. Biol.* **1500**, 51–80 (2017). doi: 10.1007/978-1-4939-6454-3; pmid: 27813001
28. S. M. Douglas, J. J. Chou, W. M. Shih, DNA-nanotube-induced alignment of membrane proteins for NMR structure determination. *Proc. Natl. Acad. Sci. U.S.A.* **104**, 6644–6648 (2007). doi: 10.1073/pnas.0700930104; pmid: 17404217
29. G. P. Acuna *et al*., Fluorescence enhancement at docking sites of DNA-directed self-assembled nanoantennas. *Science* **338**, 506–510 (2012). doi: 10.1126/science.1228638; pmid: 23112329
30. A. Kuzyk *et al*., DNA-based self-assembly of chiral plasmonic nanostructures with tailored optical response. *Nature* **483**, 311–314 (2012). doi: 10.1038/nature10889; pmid: 22422265
31. S. Douglas, I. Bachelet, G. M. Church, A logic-gated nanorobot for targeted transport of molecular payloads. *Science* **335**, 831–834 (2012). doi: 10.1126/science.1214081; pmid: 22344439
32. Z. Jin *et al*., Metallized DNA nanolithography for encoding and transferring spatial information for graphene patterning. *Nat. Commun.* **4**, 1663 (2013). doi: 10.1038/ncomms2690; pmid: 23575667
33. W. Sun *et al*., Casting inorganic structures with DNA molds. *Science* **346**, 1258361 (2014). doi: 10.1126/science.1258361; pmid: 25301973
34. J. Fu *et al*., Multi-enzyme complexes on DNA scaffolds capable of substrate channelling with an artificial swinging arm. *Nat. Nanotechnol.* **9**, 531–536 (2014). doi: 10.1038/nnano.2014.100; pmid: 24859813
35. J. B. Knudsen *et al*., Routing of individual polymers in designed patterns. *Nat. Nanotechnol.* **10**, 892–898 (2015). doi: 10.1038/nnano.2015.190; pmid: 26322946
36. P. C. Nickels *et al*., Molecular force spectroscopy with a DNA origami–based nanoscopic force clamp. *Science* **354**, 305–307 (2016). doi: 10.1126/science.aah5974; pmid: 27846560
37. F. Kilchherr *et al*., Single-molecule dissection of stacking forces in DNA. *Science* **353**, aaf5508 (2016). doi: 10.1126/science.aaf5508; pmid: 27609897
38. T. G. Martin *et al*., Design of a molecular support for cryo-EM structure determination. *Proc. Natl. Acad. Sci. U.S.A.* **113**, E7456–E7463 (2016). doi: 10.1073/pnas.1612720113; pmid: 27821763
39. A. Gopinath, E. Miyazono, A. Faraon, P. W. K. Rothemund, Engineering and mapping nanocavity emission via precision placement of DNA origami. *Nature* **535**, 401–405 (2016). doi: 10.1038/nature18287; pmid: 27398616
40. N. A. W. Bell, U. F. Keyser, Digitally encoded DNA nanostructures for multiplexed, single-molecule protein sensing with nanopores. *Nat. Nanotechnol.* **11**, 645–651 (2016). doi: 10.1038/nnano.2016.50; pmid: 27043197
41. C. Lin, M. Xie, J. J. L. Chen, Y. Liu, H. Yan, Rolling-circle amplification of a DNA nanojunction. *Angew. Chem. Int. Ed.* **45**, 7537–7539 (2006). doi: 10.1002/anie.200602113; pmid: 17048296
42. C. Lin, X. Wang, Y. Liu, N. C. Seeman, H. Yan, Rolling circle enzymatic replication of a complex multi-crossover DNA nanostructure. *J. Am. Chem. Soc.* **129**, 14475–14481 (2007). doi: 10.1021/ja0760980; pmid: 17963390
43. Z. Li *et al*., A replicable tetrahedral nanostructure self-assembled from a single DNA strand. *J. Am. Chem. Soc.* **131**, 13093–13098 (2009). doi: 10.1021/ja903768f; pmid: 19737020
44. C. Geary, P. W. Rothemund, E. S. Andersen, A single-stranded architecture for cotranscriptional folding of RNA nanostructures. *Science* **345**, 799–804 (2014). doi: 10.1126/science.1253920; pmid: 25124436
45. C. X. Lin *et al*., In vivo cloning of artificial DNA nanostructures. *Proc. Natl. Acad. Sci. U.S.A.* **105**, 17626–17631 (2008). doi: 10.1073/pnas.0805416105; pmid: 18927233
46. C. Ducani, C. Kaul, M. Moche, W. M. Shih, B. Högberg, Enzymatic production of 'monoclonal stoichiometric' single-stranded DNA oligonucleotides. *Nat. Methods* **10**, 647–652 (2013). doi: 10.1038/nmeth.2503; pmid: 23727986
47. N. C. Seeman, The design and engineering of nucleic acid nanoscale assemblies. *Curr. Opin. Struct. Biol.* **6**, 519–526 (1996). doi: 10.1016/S0959-440X(96)80118-7; pmid: 8794156
48. X. Zhang, H. Yan, Z. Shen, N. Seeman, Paranemic cohesion of topologically-closed DNA molecules. *J. Am. Chem. Soc.* **124**, 12940–12941 (2002). doi: 10.1021/ja026973b; pmid: 12405808
49. Z. Shen, H. Yan, T. Wang, N. Seeman, Paranemic crossover DNA: A generalized Holliday structure with applications in nanotechnology. *J. Am. Chem. Soc.* **126**, 1666–1674 (2004). doi: 10.1021/ja038381e; pmid: 14871096
50. D. Han, S. Jiang, A. Samanta, Y. Liu, H. Yan, Unidirectional scaffold-strand arrangement in DNA origami. *Angew. Chem. Int. Ed.* **52**, 9031–9034 (2013). doi: 10.1002/anie.201302177; pmid: 23852715
51. L. Jaeger, N. B. Leontis, Tecto-RNA: One-dimensional self-assembly through tertiary interactions. *Angew. Chem. Int. Ed.* **39**, 2521–2524 (2000). doi: 10.1002/1521-3773(20000717)39:14<2521::AID-ANIE2521>3.0.CO;2-P; pmid: 10941124
52. A. Chworos *et al*., Building programmable jigsaw puzzles with RNA. *Science* **306**, 2068–2072 (2004). doi: 10.1126/science.1104686; pmid: 15604402
53. C. J. Delebecque, A. B. Lindner, P. A. Silver, F. A. Aldaye, Organization of intracellular reactions with rationally designed RNA assemblies. *Science* **333**, 470–474 (2011). doi: 10.1126/science.1206938; pmid: 21700839
54. L. Jaeger, A. Chworos, The architectonics of programmable RNA and DNA nanostructures. *Curr. Opin. Struct. Biol.* **16**, 531–543 (2006). doi: 10.1016/j.sbi.2006.07.001; pmid: 16843653
55. J. W. Alexander, G. B. Briggs, On types of knotted curves, in *The Annals of Mathematics, Second Series* (Annals of Mathematics, 1926), pp. 562–586.
56. J. W. Alexander, Topological invariants of knots and links. *Trans. Am. Math. Soc.* **30**, 275–306 (1928). doi: 10.1090/S0002-9947-1928-1501429-1
57. K. Murasugi, *Knot Theory and Its Applications* (Springer Science and Business Media, 2007).
58. M. L. Mansfield, Are there knots in proteins? *Nat. Struct. Mol. Biol.* **1**, 213–214 (1994). doi: 10.1038/nsb0494-213; pmid: 7656045
59. F. Takusagawa, S. Kamitori, A real knot in protein. *J. Am. Chem. Soc.* **118**, 8945–8946 (1996). doi: 10.1021/ja961147m
60. W. R. Taylor, A deeply knotted protein structure and how it might fold. *Nature* **406**, 916–919 (2000). doi: 10.1038/35022623; pmid: 10972297
61. J. R. Wagner, J. S. Brunzelle, K. T. Forest, R. D. Vierstra, A light-sensing knot revealed by the structure of the

Downloaded from https://www.science.org on November 16, 2023

chromophore-binding domain of phytochrome. *Nature* **438**, 325–331 (2005). doi: 10.1038/nature04118; pmid: 16292304

62. H. Lee, E. Popodi, H. Tang, P. L. Foster, Rate and molecular spectrum of spontaneous mutations in the bacterium *Escherichia coli* as determined by whole-genome sequencing. *Proc. Natl. Acad. Sci. U.S.A.* **109**, E2774–E2783 (2012). doi: 10.1073/pnas.1210309109; pmid: 22991466
63. M. Wang *et al.*, Autodesk Molecule Viewer; https://moleculeviewer.lifesciences.autodesk.com (2017).
64. S. Horiya *et al*., RNA LEGO: Magnesium-dependent formation of specific RNA assemblies through kissing interactions. *Chem. Biol.* **10**, 645–654 (2003). doi: 10.1016/S1074-5521(03)00146-7; pmid: 12890538
65. More formally, previous scaffolded origami work and the DNA brick work demonstrate the construction of a size n object using $O(n)$ number of components; the unimolecular ssOrigami demonstrates the construction of a size n object using one component; the two-strand case represents its construction using $O(1)$ components; the 20-strand case represents its construction using $O(\sqrt{n})$ components.
66. S. Williams, K. Lund, C. Lin, P. Wonka, S. Lindsay, H. Yan, Tiamat: A three-dimensional editing tool for complex DNA structures, in *International Workshop on DNA-Based Computers* (Springer, 2008), pp. 90–101.

ACKNOWLEDGMENTS

The authors thank W. Shih and P. Rothemund for helpful discussions. B.A. thanks A. Berliner, E. Groban, J. Schaeffer, F. Mazzoldi, A. Kimoto, L. Peck, and M. Tinnus for help with software tool development. The work was funded by Office of Naval Research grants N000141010827, N000141310593, N000141410610, N000141612182, and N000141612410; Army Research Office grant W911NF1210238; National Science Foundation grants CCF1054898, CMMI1333215, CMMI1334109, CMMI1344915, and CCF1317291; and National Institutes of Health grant 1R01EB01865901 to P.Y.; Office of Naval Research grant N000141512689 and NSF grants 1360635, 1563799, and 1334109 to H.Y.; and internal support from Autodesk Life Sciences. B.W. thanks the China Scholarship Council (No.201506340048) for fellowship support. C.M. was funded by the Fannie and John Hertz Foundation. All data are reported in the main text and in the Supplementary Materials. A provisional U.S. patent has been filed based on this work. P.Y. is cofounder of Ultivue Inc. and NuProbe Global.

SUPPLEMENTARY MATERIALS

www.sciencemag.org/content/358/6369/eaao2648/suppl/DC1
Supplementary Text
Figs. S1-1 and S1-2, S2-1 and S2-2, S3-1 to S3-5, S4-1 to S4-8, S5-1 to S5-12, S6-1 to S6-3, S7-1 to S7-4, S8, S9-1 and S9-2, S10-1 to S10-3, S11-1 to S11-9, S12-1 to S12-22
References (*67*, *68*)
Movies S1 to S16

1 July 2017; accepted 27 October 2017
10.1126/science.aao2648

Downloaded from https://www.science.org on November 16, 2023

Science
AAAS

Single-stranded DNA and RNA origami

Dongran Han, Xiaodong Qi, Cameron Myhrvold, Bei Wang, Mingjie Dai, Shuoxing Jiang, Maxwell Bates, Yan Liu, Byoungkwon An, Fei Zhang, Hao Yan, and Peng Yin

Science **358** (6369), eaao2648. DOI: 10.1126/science.aao2648

Large origami from a single strand

Nanostructures created by origami-like folding of nucleic acids are usually formed by base-pairing interactions between multiple strands. Han *et al.* show that large origami (up to 10,000 nucleotides for DNA and 6000 nucleotides for RNA) can be created in simple shapes, such as a rhombus or a heart. A single strand can be folded smoothly into structurally complex but knot-free structures by using partially complemented double-stranded DNA and the cohesion of parallel crossovers. The use of single strands also enables in vitro synthesis of these structures.

Science, this issue p. eaao2648

View the article online
https://www.science.org/doi/10.1126/science.aao2648
Permissions
https://www.science.org/help/reprints-and-permissions

Downloaded from https://www.science.org on November 16, 2023

Use of this article is subject to the Terms of service

Science (ISSN 1095-9203) is published by the American Association for the Advancement of Science. 1200 New York Avenue NW, Washington, DC 20005. The title *Science* is a registered trademark of AAAS.

Copyright © 2017 The Authors, some rights reserved; exclusive licensee American Association for the Advancement of Science. No claim to original U.S. Government Works